International Journal of Heat and Mass Transfer 52 (2009) 1753–1760

Contents lists available at ScienceDirect

International Journal of Heat and Mass Transfer

journal homepage: www.elsevier.com/locate/ijhmt

An enhanced thermal conduction model for the prediction of convection dominated solid–liquid phase change

Guillaume Vidalain [a], Louis Gosselin [a,*], Marcel Lacroix [b]

[a] Département de génie mécanique, Université Laval, Québec, Que., Canada G1K 7P4
[b] Département de génie mécanique, Université de Sherbrooke, Sherbrooke, Que., Canada J1K 2R1

ARTICLE INFO

Article history:
Received 12 May 2008
Received in revised form 11 September 2008
Available online 4 December 2008

Keywords:
Solid–liquid phase change
Enhanced thermal conductivity
Phase change material (PCM)
Melting and solidification
Furnace
Latent heat energy storage

ABSTRACT

An enhanced thermal conduction model for predicting convection dominated solid–liquid phase change is presented. The main feature of the model is to predict (1) the overall thermal behavior of the system and (2) the phase front position without recurring to the full solution of the Navier–Stokes equations. The model rests entirely on the conduction equation for both the solid and liquid phases. The effect of convection in the melt is mimicked via an enhanced thermal conductivity that depends on the dimensionless numbers and the geometry of the flow. The model is tested and confronted to full CFD solutions for a freezing duct flow problem and for buoyancy driven melting in an enclosure. In both cases, the predictions of the enhanced thermal conduction model show excellent agreement with that of the CFD model. Not only is the enhanced thermal conduction model simpler to implement but its simulations run at least ten times as fast as those of the CFD model. Consequently, the enhanced thermal conduction model is well suited for controlling real-time solid–liquid phase change processes that occur in industrial applications as well as in latent heat thermal energy storage systems.

1. Introduction

For more than two decades now, convection dominated solid–liquid phase change problems have been the subject of many investigations in the open literature. The interest for these problems stems from their wide range of applications, chiefly in metallurgy and material processing and in latent heat energy storage systems. Recent work in these fields is reported in Refs. [1–10].

Numerical simulation of convection dominated phase change problems is a challenging task. Not only are these problems strongly nonlinear, i.e., the fluid flow in the melt dictates the heat transfer, but they also involve moving boundaries, i.e., the solid–liquid interface. Since the heat transfer coefficient at the moving front is, in general, not known, the coupled energy equations in the solid and liquid phases, together with the conservation equations of mass and momentum in the melt, must be solved. As a result, even the numerical solution for the simplest convection dominated phase change problem involves complex and time-consuming calculations (see the review of Hu and Argyropoulos [11]). Different numerical approaches are available for solving the heat transfer and fluid flow during solid–liquid phase change. These strategies rest on either interface tracking methods (moving grids) or on enthalpy methods (fixed grids) [12–14]. Sometimes however, performing these lengthy calculations is simply impractical. This is the case, for instance, when one envisages to control high temperature melting furnaces over long periods of time [8] or to predict the thermal behavior of latent heat thermal energy storage systems that are operated cyclically [9]. It is obvious that in these real-time situations, the complete picture of the flow field is not required and that the computational procedure must be simplified in order to provide quick results to be fed back to the control system.

One interesting way to simplify the computational procedure is to abandon the calculation of the melt flow (i.e., the mass and the momentum equations are no longer solved) and to account for the effect of convection in the melt via an enhanced thermal conductivity in the energy equation [15]. This approach has been employed in the past for predicting the thermal behavior of melting furnaces and that of energy storage systems [7–9].

In spite of the success of this strategy, none of the above studies has addressed the question of how to choose the appropriate enhanced thermal conductivity. In fact, most of the time, the melt conductivity is simply adjusted empirically so as to match the numerical predictions with the experimental data.

The present paper addresses this question. It is shown that the enhanced thermal conductivity of the melt may be formulated in terms of directional thermal conductivity components and that their values may be correlated in terms of dimensionless numbers obtained from an order of magnitude analysis. The proposed approach is then tested for two different test cases. The first test case

* Corresponding author. Tel.: +1 418 656 7829; fax: +1 418 656 7415.
E-mail address: Louis.Gosselin@gmc.ulaval.ca (L. Gosselin).

0017-9310/$ - see front matter © 2008 Elsevier Ltd. All rights reserved.
doi:10.1016/j.ijheatmasstransfer.2008.09.020

Nomenclature

A_{mush}	mushy zone constant
c_p	heat capacity, J kg^{-1} K^{-1}
D	spacing, m
H	height, m
f	liquid fraction
g	gravitational acceleration, m s^{-2}
h	heat transfer coefficient, W m^{-2} K^{-1}
k	thermal conductivity, W m^{-1} K^{-1}
k'	directional pseudo-thermal conductivity associated with convection, W m^{-1} K^{-1}
L	length, m
Nu	Nusselt number
Pe	Péclet number
Pr	Prandtl number
q	heat transfer rate, W
Ra	Rayleigh number
s	solid–liquid interface position, m
S_f	source term
Ste	Stefan number
t	time, s
T	temperature, K
T'	temperature fluctuation, K
u, v, w	velocity components, m s^{-1}
v'	velocity fluctuation, m s^{-1}
U	inlet velocity, m s^{-1}
x, y, z	Cartesian coordinates, m

Greek symbols

α	thermal diffusivity, m^2 s^{-1}
β	coefficient of thermal expansion, K^{-1}
γ	small number
ε_H	eddy thermal diffusivity, m^2 s^{-1}
λ	latent heat, J kg^{-1}
ν	dynamic viscosity, m^2 s^{-1}
ρ	density, kg m^{-3}
η	algebraic coefficient

Subscripts

bc	cold
en	enhanced
h	hot
L	liquidus
m	melting
S	solidus
w	wall
x, y, z	direction
∞	inlet

Superscripts

$\sim$	dimensionless quantity
$\bar{}$	average

is devoted to forced convection dominated solidification in a duct while the second test case is concerned with buoyancy dominated melting in an enclosure.

2. Mathematical formulation and closure problem

In the following section, the fundamentals of the enhanced conductivity approach are derived for a laminar flow. We begin by gathering the convection terms in the energy equation along with the conduction terms in the following way:

$$\rho c_p \frac{\partial T}{\partial t} = \frac{\partial}{\partial x}\left(k\frac{\partial T}{\partial x} - \rho c_p u T\right) + \frac{\partial}{\partial y}\left(k\frac{\partial T}{\partial y} - \rho c_p v T\right) + \frac{\partial}{\partial z}\left(k\frac{\partial T}{\partial z} - \rho c_p w T\right) + S_f \quad (1)$$

S_f is a source term that accounts for the latent heat released or absorbed when phase change takes place. For instance, in the well-known phase change porosity-enthalpy method [1], S_f reads as

$$S_f = -\rho\lambda\left(u\frac{\partial f}{\partial x} + v\frac{\partial f}{\partial y} + w\frac{\partial f}{\partial z} + \frac{\partial f}{\partial t}\right) \quad (2)$$

where the local liquid fraction f is defined as

$$f = \begin{cases} 0 & T < T_S \\ \left(\frac{T-T_S}{T_L-T_S}\right) & T_S < T < T_L \\ 1 & T > T_L \end{cases} \quad (3)$$

The term S_f is non-zero only in the mushy zone, i.e., in the region where latent heat is released or absorbed. The terms of the form $k(\partial T/\partial j) - \rho c_p u_j T$ (with $j = x, y, z$) in Eq. (1) represent the net energy flow in the j-direction and can be related in 2D to the so-called heat function [16,17].

The next conceptual step is to recognize that, in some cases, we may not be concerned with the exact velocity and pressure profiles in the melt. This is especially true in problems for which only the overall thermal behavior of the system is sought or in problems for which only the knowledge of the solid–liquid interface position is required (e.g., melting furnace, latent heat storage system). Therefore, we rewrite Eq. (1) as

$$\rho c_p \frac{\partial T}{\partial t} = \frac{\partial}{\partial x}\left((k + k'_x)\frac{\partial T}{\partial x}\right) + \frac{\partial}{\partial y}\left(\left(k + k'_y\right)\frac{\partial T}{\partial y}\right) + \frac{\partial}{\partial z}\left((k + k'_z)\frac{\partial T}{\partial z}\right) + S_f \quad (4)$$

The directional thermal conductivities associated with convection in the x, y, and z directions, i.e., k'_x, k'_y and k'_z, are defined as

$$k'_x = \left|\frac{\rho c_p u T}{\partial T/\partial x}\right| \quad k'_y = \left|\frac{\rho c_p v T}{\partial T/\partial y}\right| \quad k'_z = \left|\frac{\rho c_p w T}{\partial T/\partial z}\right| \quad (5)$$

In the solid phase, the velocity components are zero, and consequently $k'_x = k'_y = k'_z = 0$.

For a better understanding of the fundamentals of the enhanced conductivity approach, it is instructive to recall that the above formulation is akin to that of the time-averaged conservation equations for turbulent flows [16]. The eddy thermal diffusivity that appears in the energy equation for turbulent flows is a function of the local fluctuations in the temperature and in the velocity components. For example, the eddy diffusivity in a thermal boundary layer is $\varepsilon_H = -\overline{v'T'}/(\partial\bar{T}/\partial y)$ [16]. The closure problem is then to find the relation between the averaged fluctuations and the time-averaged dependent variables. This is the realm of turbulence modeling. Based on experimental observation [16], Prandtl's mixing length approach yields an algebraic model for the thermal eddy diffusivity of the form $\varepsilon_H = -K^2y^2|\partial\bar{T}/\mathrm{d}y|$, where K is an empirical constant of order 1. This model is simple and has been applied successfully to a wide range of boundary layer flows. It is, however, dependent on the geometry and it fails to provide accurate results when the flow separates from the

wall. More general turbulence models such as the $k-\varepsilon$ model are available but they are more complex and they involve the solution of time-consuming nonlinear differential equations.

It is assumed, in the present study, that the directional thermal conductivities associated with convection (k'_x, k'_y, and k'_z) play a role similar to that of the eddy diffusivity in turbulence modeling. The problem then is to find a relation between the directional conductivities and the geometry of the flow. To achieve this goal, Prandtl's approach is retained. A simple algebraic model, based on a scale analysis, is first proposed and its empirical constants are determined with precision from CFD simulations and experimental data. The main steps of the overall strategy are summarized in Fig. 1. Once the algebraic relations are established, they can be used straightforwardly in a wide range of situations.

Before presenting the test cases, we emphasize the fact that the enhanced conduction approach is a numerical method for performing quick calculations of convection dominated heat transfer problems. It is not a substitute for CFD calculations. The enhanced conduction approach provides an estimate of the overall thermal behavior of systems and as a result, it is well suited for controlling real-time solid–liquid phase change processes that occur in industrial applications.

3. Test case 1: freezing duct flow

To illustrate the utilization of the enhanced conduction model in convection dominated phase change problems, we first consider the simple case of laminar freezing flow in a duct, as shown in Fig. 2. A phase change fluid (here, we consider the molten metal gallium) at temperature T_∞ enters a channel of height H and length L at a velocity U_∞. The solidification temperature of the fluid is T_s and the walls of the channel are maintained at a temperature T_w ($T_w < T_s < T_\infty$). As heat is lost through the boundaries, a solid layer grows on the walls. The problem that we address here is to predict the time evolution of the solid–liquid interface. This is done first, with a full CFD model and, second, with the proposed enhanced conduction model. Both models are presented in the following sub-sections and their predictions are confronted in Section 4.

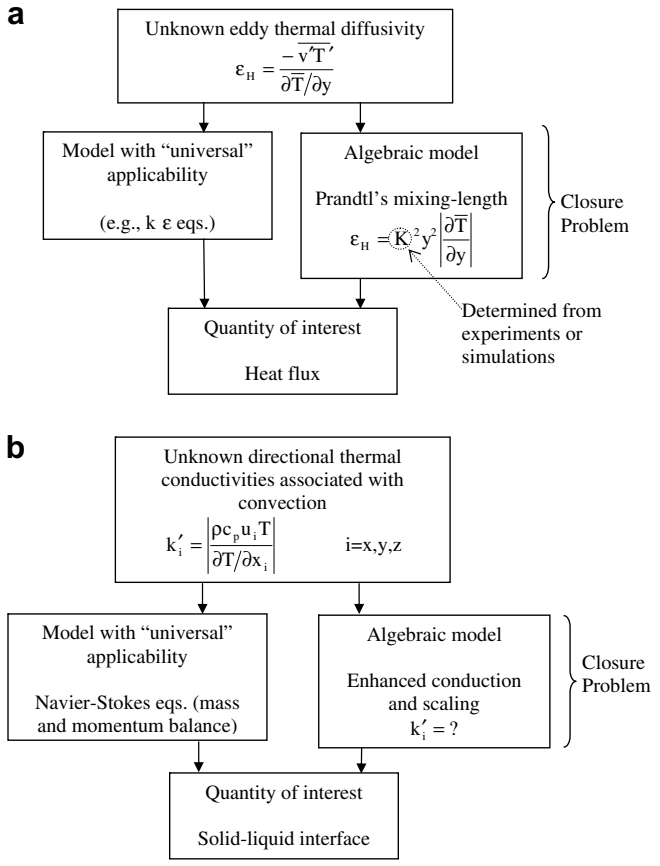

Fig. 1. Comparison between the modeling of (a) turbulence and (b) phase change problems.

3.1. CFD model

In the CFD model, the flow is determined by solving the complete set of Navier–Stokes equations. The results of the CFD model are then used as a basis of comparison for the enhanced thermal conduction model described in Section 3.2.

Assuming that the fluid is Newtonian with constant properties and that the flow is laminar, the mass, momentum and energy equations for the CFD model may be stated as

$$\frac{\partial\tilde{u}}{\partial\tilde{x}}+\frac{\partial\tilde{v}}{\partial\tilde{y}}=0 \tag{6}$$

$$\frac{\mathrm{Pe}_L}{\mathrm{Pr}}\left(\frac{\partial\tilde{u}}{\partial\tilde{t}}+\tilde{u}\frac{\partial\tilde{u}}{\partial\tilde{x}}+\tilde{v}\frac{\partial\tilde{u}}{\partial\tilde{y}}\right)=-\frac{\mathrm{Pe}_L}{\mathrm{Pr}}\frac{\partial\tilde{p}}{\partial\tilde{x}}+\frac{\partial^2\tilde{u}}{\partial\tilde{x}^2}+\frac{\partial^2\tilde{u}}{\partial\tilde{y}^2}+\tilde{S}_A\tilde{u} \tag{7}$$

$$\frac{\mathrm{Pe}_L}{\mathrm{Pr}}\left(\frac{\partial\tilde{v}}{\partial\tilde{t}}+\tilde{u}\frac{\partial\tilde{v}}{\partial\tilde{x}}+\tilde{v}\frac{\partial\tilde{v}}{\partial\tilde{y}}\right)=-\frac{\mathrm{Pe}_L}{\mathrm{Pr}}\frac{\partial\tilde{p}}{\partial\tilde{y}}+\frac{\partial^2\tilde{v}}{\partial\tilde{x}^2}+\frac{\partial^2\tilde{v}}{\partial\tilde{y}^2}+\frac{\mathrm{Ra}_L}{\mathrm{Pe}_L}\tilde{T}+\tilde{S}_A\tilde{v} \tag{8}$$

$$\mathrm{Pe}_L\left(\frac{\partial\tilde{T}}{\partial\tilde{t}}+\tilde{u}\frac{\partial\tilde{T}}{\partial\tilde{x}}+\tilde{v}\frac{\partial\tilde{T}}{\partial\tilde{y}}\right)=\frac{\partial^2\tilde{T}}{\partial\tilde{x}^2}+\frac{\partial^2\tilde{T}}{\partial\tilde{y}^2}+\tilde{S}_f \tag{9}$$

where Pr is the Prandtl number ($\mathrm{Pr}=\nu/\alpha=0.018$ for gallium) and Pe_L is the Péclet number ($\mathrm{Pe}_L=U_\infty L/\alpha$). The other dimensionless variables and numbers are defined as

$$\tilde{x},\tilde{y}=\frac{x,y}{L}\quad \tilde{u},\tilde{v}=\frac{u,v}{U_\infty}\quad \tilde{t}=\frac{t}{L/U_\infty}\quad \tilde{p}=\frac{p}{\rho U_\infty^2}\quad \tilde{T}=\frac{T-T_w}{T_m-T_w} \tag{10}$$

$$\mathrm{Ra}_L=\frac{g\beta(T_m-T_w)L^3}{\nu\alpha}\quad \mathrm{Ste}=\frac{c_p(T_m-T_w)}{\lambda}\quad \tilde{S}_f=\frac{1}{\mathrm{Ste}}S_f$$

$$\tilde{S}_A=\frac{L(1-f^2)A_{mush}}{\rho U_\infty(f^3-\gamma)} \tag{11}$$

Note that for the freezing duct flow problem, natural convection is neglected, i.e., Ra = 0 in Eq. (8).

The source terms $\tilde{S}_A$ in the momentum Eqs. (7) and (8) are used to drive the velocity components to zero inside the solid phase. The latent heat stored or released during phase change is accounted for via the source term $\tilde{S}_f$ in the energy Eq. (9). The dimensionless temperature at the walls is set at $\tilde{T}=0$. The inlet temperature is fixed at 2 and the solidification temperature is fixed at 1. A uniform velocity profile is imposed at the inlet while the no-slip boundary condition is invoked at the walls.

The above set of differential equations was discretized using a finite-volume method [18] and the resulting sets of algebraic equations were solved numerically with a commercial CFD package [19]. Convergence, at a given time step, was declared when the residuals, for each conservation equation, had decreased by 4 orders of magnitude (6 for the energy equation).

The computational procedure was tested for grid and time step independence. The mesh was refined until further grid density doubling resulted in overall liquid fraction $\bar{f}$ that differ by less than 1% from mesh i to mesh $i+1$, i.e.,

$$\left|\frac{\bar{f}_{i+1}-\bar{f}_i}{\bar{f}_i}\right|<1\% \tag{12}$$

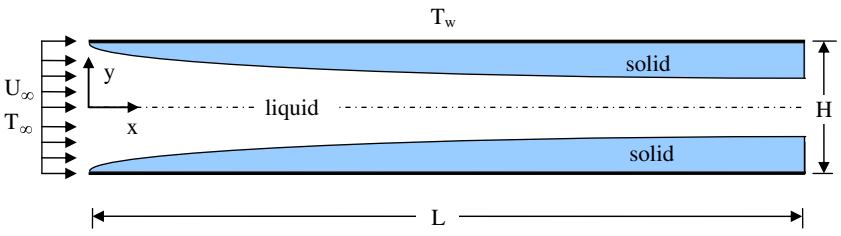

Fig. 2. Schematic representation of a channel flow with solidification on the walls.

Table 1
An example of mesh independence study for the complete CFD model ($H/L = 0.6$).

Mesh	$Re_L = Pe_L/Pr = 1000$		$Re_L = Pe_L/Pr = 2000$		$Re_L = Pe_L/Pr = 3800$	
	$\bar{f}_i$	$\lvert(\bar{f}_i - \bar{f}_{i-1})/\bar{f}_i\rvert$ (%)	$\bar{f}_i$	$\lvert(\bar{f}_i - \bar{f}_{i-1})/\bar{f}_i\rvert$ (%)	$\bar{f}_i$	$\lvert(\bar{f}_i - \bar{f}_{i-1})/\bar{f}_i\rvert$ (%)
20 × 6	0.595	–	0.731	–	0.799	–
40 × 12	0.534	11.50	0.647	12.86	0.736	8.583
80 × 24	0.503	6.05	0.617	4.89	0.693	6.258
160 × 48	0.476	5.73	0.601	2.72	0.681	1.722
320 × 96	0.456	4.52	0.594	1.11	0.677	0.516
640 × 92	–	–	0.593	0.27	0.679	0.325

Similarly, the time step was varied until further time step reduction resulted in overall liquid fraction changes smaller than 1%. A mesh comprising 320 × 96 cells and a dimensionless time step of 0.1 were found to satisfy these requirements for the range of Peclet numbers and H/L ratios considered in this study (see Table 1).

3.2. Enhanced thermal conduction model

In the enhanced thermal conduction model, convection heat transfer in the melt is mimicked via an augmented thermal conductivity. Referring to Section 2, the parameter that characterizes this model is the ratio of the x to y-overall directional conductivity components:

$$\tilde{k}_{en} = \frac{k + k'_x}{k + k'_y} \tag{13}$$

In view of Eq. (5) and of the geometry shown in Fig. 2, the correct scale for the x- conductivity associated with convection in the x direction is $k'_x \sim \rho c_p U_\infty L$ where $k'_y << k'_x$. Both, the thermal and the velocity boundary layers grow on the walls. Since Pr << 1, the thermal boundary layer is much thicker. As a result, $v \to 0$ in most of the melt and hence $k'_y \to 0$. Thus, the enhanced thermal conductivity ratio in Eq. (13) is expected to scale as

$$\tilde{k}_{en} \sim 1 + \frac{U_\infty L}{\alpha} = 1 + Pe_L \tag{14}$$

$\tilde{k}_{en}$ is proportional to the Péclet number of the flow for thin banks. However, as the cross-section of the channel decreases, the ratio of the thickness of the solid layer to the channel height increases and, from the mass conservation principle, the x-velocity scale in the channel becomes larger than U_∞. As a result, $s/H \sim Pe_L^{-1/2}/(H/L)$ and $u \sim U_\infty H/s$ and the enhanced thermal conductivity may be rewritten as

$$\tilde{k}_{en} \sim 1 + \frac{Pe_L^{1/2}}{H/L} = \eta_1 + \eta_2 \frac{Pe_L^{1/2}}{H/L} \tag{15}$$

where η_1 and η_2 are constants of order 1, i.e., $\eta_1, \eta_2 = O(1)$, similar to the constant K in Prandtl's algebraic turbulence model (see Fig. 1). Eq. (14) holds for channels with large breadth, while Eq. (15) is expected to be more general.

Based on the aforementioned assumptions, Eq. (4) reduces to

$$Pe_L \frac{\partial \tilde{T}}{\partial \tilde{t}} = \tilde{k}_{en} \frac{\partial^2 \tilde{T}}{\partial \tilde{x}^2} + \frac{\partial^2 \tilde{T}}{\partial \tilde{y}^2} + \tilde{S}_f \tag{16}$$

Solutions of this simple diffusion equation can be sought provided that $\tilde{k}_{en}$ can be estimated, for example with Eq. (14) or Eq. (15). In the next section, we validate the scale analysis presented above, and determine the best values for the constants η_1 and η_2.

4. Results for the freezing duct flow problem

A series of numerical simulations was carried out with the CFD model for Péclet numbers ranging from 20 to 80 and for aspect ratios of the channel (H/L) ranging from 0.3 to 0.9. These ranges for

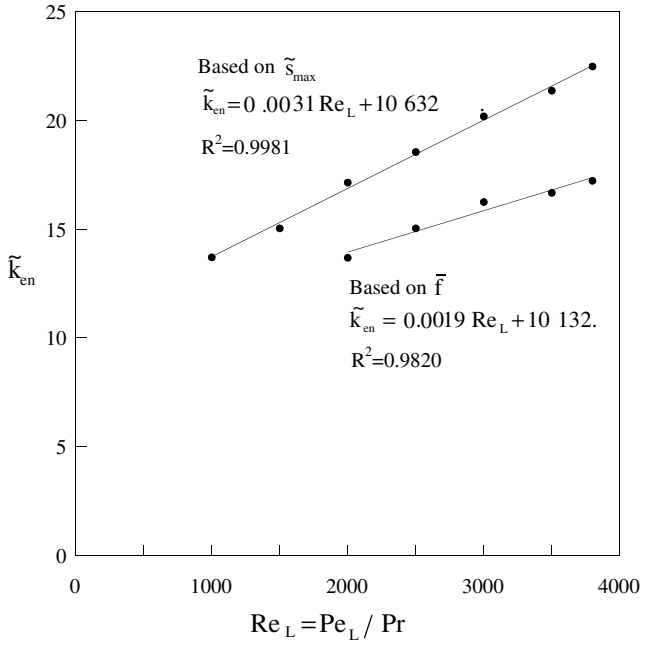

Fig. 3. Predicted $\tilde{k}_m$ values for matching the predictions of the enhanced conduction model with those of the CDF model.

the Pe numbers and H/L ratios guarantee a laminar flow in the duct.

Similar calculations were performed with the enhanced conduction model so as to determine the $\tilde{k}_{en}$-values that yield maximum solid layer thickness $\tilde{s}_{max}$ and mean liquid fraction $\bar{f}$ that match the predictions of the CDF model. As an example, the variation of the required $\tilde{k}_{en}$-values in terms of the Reynolds number for an aspect ratio $H/L = 0.6$ is shown in Fig. 3. Each dot represents the result of a CFD simulation and the curves are linear regressions based on these points. One curve is based on the $\tilde{s}_{max}$ values while the other rests on the $\bar{f}$ values. Both curves depict a nearly linear relation between $\tilde{k}_{en}$ and Re, as expected from Eq. (14).

The predicted time evolution of the mean liquid fraction $\bar{f}$ is shown in Fig. 4. It is seen that the predictions of the enhanced conduction model and that of the CFD simulations are in very good agreement. These results show that the enhanced conduction model can handle adequately the convection dominated freezing duct flow.

One can argue that the enhanced conduction model requires the use of a CFD code for determining $\tilde{k}_{en}$. In fact, as we have seen (see Eq. (15)), the scale for $\tilde{k}_{en}$ can actually be predicted without recurring to CFD. The adjustment of the constants η_1 and η_2 simply improves the accuracy of the results. In the present study, it was found that the $\tilde{k}_{en}$-values of Eq. (15) were best correlated with

$$\eta_1 = 5.2 \quad \text{and} \quad \eta_2 = 1.1 \tag{17}$$

The R^2-factor of the fitting is 0.97. Moreover, it is seen that η_1 and η_2 are truly of order 1. Therefore, in spite of its relative simplicity, the scaling method proposed in Section 3 provides satisfactory results for the convection dominated freezing duct flow problem.

Incidentally, in order to reach a steady state solution, a typical enhanced conduction model simulation performed on a Pentium 3.2 GHz, 1 Go RAM runs approximately 10 times faster than a full CFD simulation.

5. Test case 2: melting inside an enclosure

The enhanced conduction model was next challenged with the problem of natural convection dominated melting shown in Fig. 5. A phase change material (PCM) is contained in a two-dimensional rectangular cavity of height H and length L. The temperature of the PCM is initially slightly lower than its melting temperature. The horizontal walls of the enclosure are adiabatic. At time $t = 0$, the temperature of the left wall is raised impulsively to a prescribed temperature above the fusion point $T_w > T_s$. As a result, melting of the PCM is triggered. At first, heat transfer in the melt zone is dominated by conduction. The solid–liquid interface moves to the right while remaining flat. But soon, buoyancy-driven convection sets in and more melting takes place in the vicinity of the top wall. The solid–liquid interface becomes distorted.

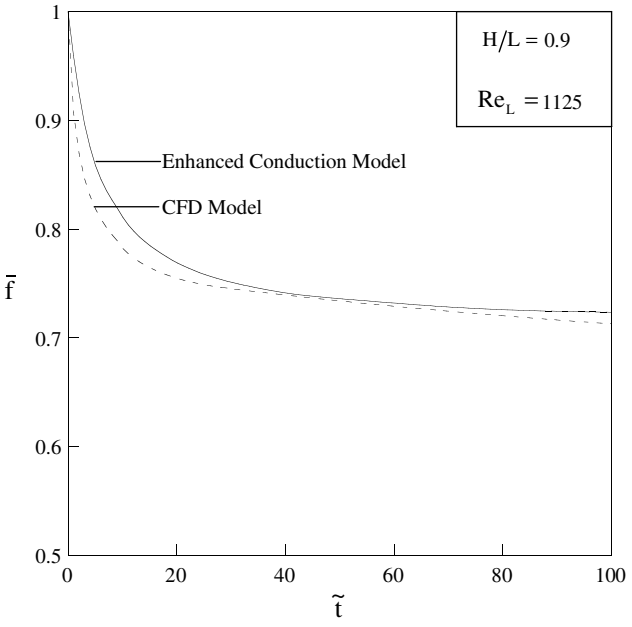

Fig. 4. Time evolution of the averaged liquid fraction predicted by the enhanced conduction model and by the CFD model.

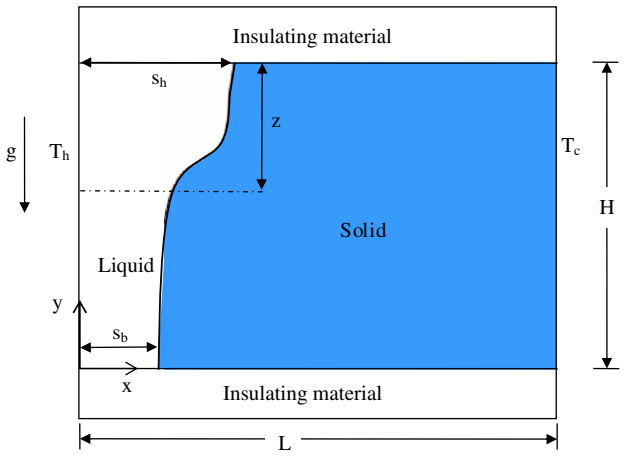

Fig. 5. Schematic representation of a cavity filled with a phase change material heated from the side wall.

This problem was retained due to the fact that it has been studied extensively in the past and has been used as a benchmark for comparing numerical methods [20]. A scale analysis is presented in Ref. [21] and experimental data are available for the melting of gallium with $H = 6.35$ cm, $L = 8.89$ cm, $T_h = 311$ K, $T(t = 0) = T_c = 301.3$ K [22,23].

Simulations of this melting problem were carried out with the same CFD code used in test case 1. The accuracy of the computations was investigated by performing grid and time step refinement studies. Simulations were finally performed with a grid size comprising 32×42 control volumes and a time step of 0.1 s similar to the parameters reported in Ref. [7].

The strategy retained to augment the conductivity is summarized in Fig. 6. It is observed that initially, heat transfer in the melt is dominated by conduction, and therefore, no modification of the conductivity is required. According to Bejan [16,21], convection in the upper left corner appears when the boundary layer thickness δ_z becomes of the same order of magnitude as the thickness of the molten layers, i.e., when $\delta_z \sim s$, as shown in Fig. 5. Here, z is the height of the convective zone in the upper region of the melt layer. Considering that $\delta_z \sim z(\mathrm{Ra}_z\mathrm{Pr})^{-1/4}$ for a fluid with $\mathrm{Pr} \ll 1$ such as gallium, it follows that when $\delta_z \sim s$, z scales as

$$\frac{z}{H} \sim \left(\frac{s}{H}\right)^4 \mathrm{Ra}_H \mathrm{Pr} \tag{18}$$

As a result, Eq. (18) may be used as a criterion to determine when the convective effects should be included in the model. For $z/H < 1$, i.e., for $\delta_z < s$, heat transfer is dominated by conduction, and there is no need to enhance the thermal conductivity. On the other hand, for $z/H \sim 1$, convection is triggered and the melt thermal conductivity is augmented accordingly.

The enhancement of k is performed in a $z \times z$ squared-shaped domain located in the upper left corner of the domain which is

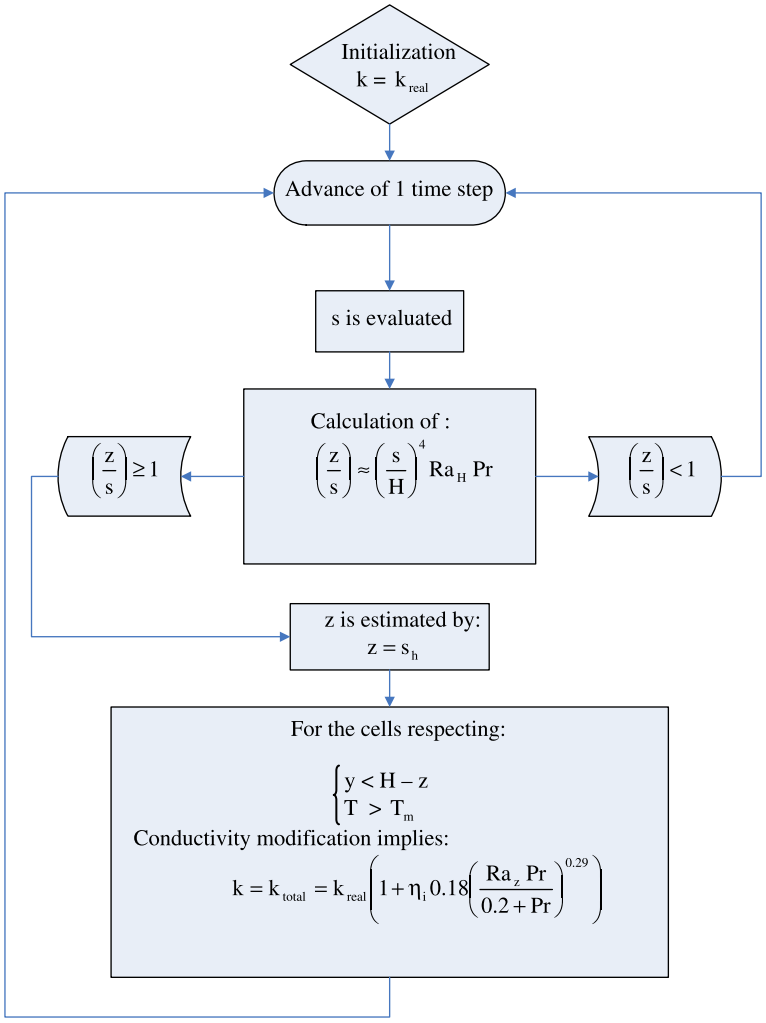

Fig. 6. Strategy for predicting the moving solid–liquid interface with the enhanced conduction model.

equivalent to the so-called "convective zone" in Ref. [21]. The modified value of k was chosen so as to mimic the heat flux due to natural convection in a $z \times z$ cavity, i.e $q'' = k'\Delta T/z = \bar{h}\Delta T$. The value of $\bar{h}$ can be estimated with an appropriate correlation for cavities such as [24],

$$\overline{\mathrm{Nu}}_z = 0.18\left(\frac{\mathrm{Pr}}{0.2+\mathrm{Pr}}\mathrm{Ra}_z\right)^{0.29} \tag{19}$$

which results in an enhanced conductivity of the form

$$k_{\mathrm{en}} \sim k(1+\overline{\mathrm{Nu}}_z) \quad \text{or} \quad k_{\mathrm{en}} = k(1+\eta\overline{\mathrm{Nu}}_z) \tag{20}$$

where η is a constant of order 1, $\eta \sim \mathrm{O}(1)$, similar to the constant K in turbulence modeling (see Fig. 1). Note that the actual value of the enhanced conductivity k_{en} depends on z, which, in turn, is a function of time. Therefore, k_{en} needs to be updated at every time step. For simplicity, it is assumed here that the dimension of the convective zone is equal to the thickness of the melt layer evaluated at the top of the cavity, i.e., $z = s(y = H)$. Note that if the simulations were to be performed at later times, that is when the conduction zone at the bottom left of the cavity has vanished completely, the height of the convective zone would become $z = H$ and z would be replaced by H in the Eqs. (18) and (19) for the calculation of the enhanced conductivity. Here the calculations were conducted in the mixed regime, i.e., the conduction zone at the bottom of the cavity was present at all time.

Simulations performed with η set equal to 1 where found to be satisfactory, i.e., the predictions of the enhanced conduction model showed a maximum discrepancy of the molten volume fraction of less than 5% with those of the full CFD predictions. Improved results were however achieved with an adjusted η-value slightly larger than one. For instance, the resulting transient solid–liquid interface positions predicted with $\eta = 1.25$ are exemplified in Fig. 7. It is seen that these results closely match those obtained with the CFD model. In particular, the distortion of the solid–liquid interface in the upper region of the cavity is well captured by the enhanced conduction model, a feature that a constant conductivity model could not simulate. The main discrepancy between the moving fronts appears at the bottom of the melt, a region where the enhanced conduction model does not apply. Once again, the computer simulations conducted with the enhanced conduction model run at least 10 times faster than those of the full CFD simulations.

The corresponding time evolution of the mean liquid fraction is depicted in Fig. 8a. This figure reveals a maximum discrepancy of 4% between the predictions of the enhanced conduction model and the CFD results. Similar observations can be made concerning the time wise variation of the heat flux at the left boundary (Fig. 8b).

Finally, let us mention that the ability of the enhanced conduction model for predicting natural convection dominated melting

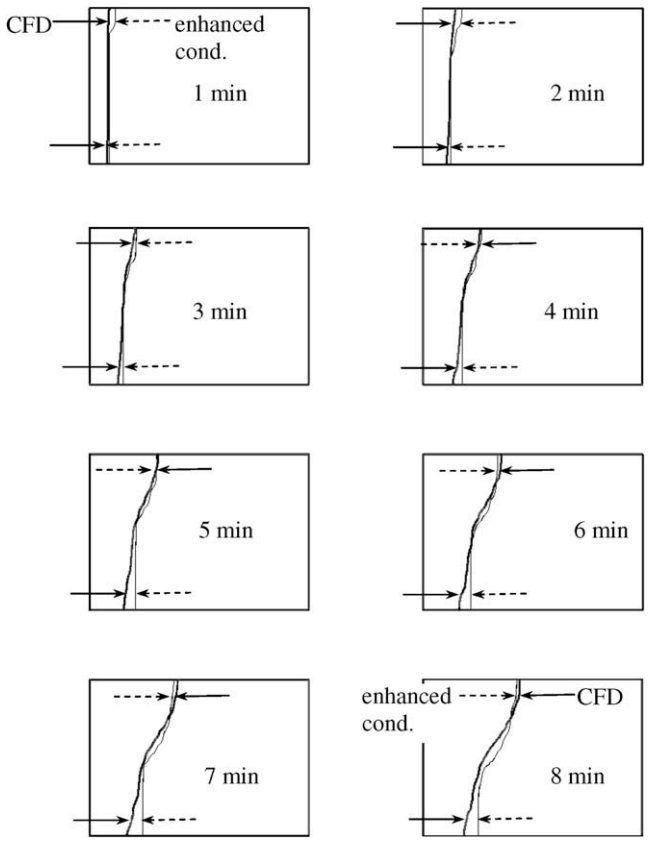

Fig. 7. Predicted solid–liquid interface positions obtained with the enhanced conduction model (broken line) and with the CFD model (solid line).

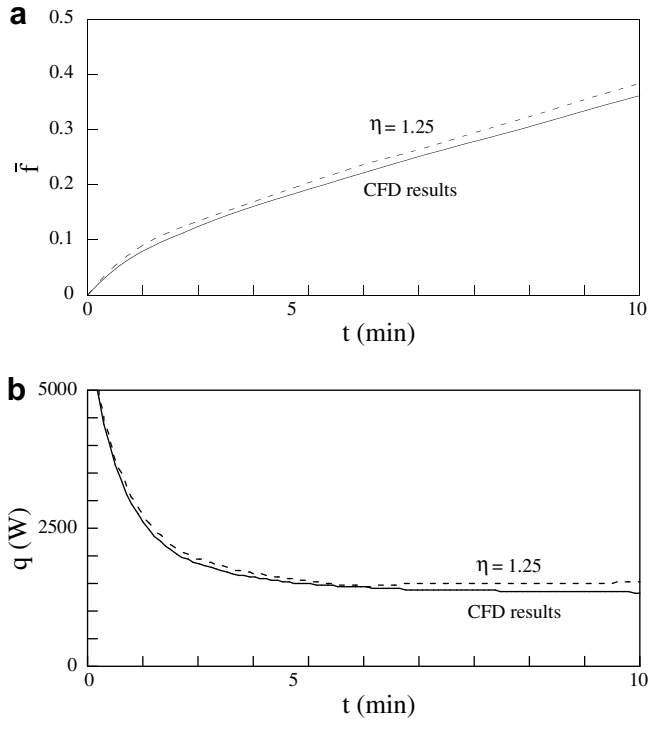

Fig. 8. Time variation of the (a) molten volume fraction and (b) heat transfer rate at the left vertical wall. Enhanced conduction model (broken line); CFD results (full line).

was tested for other sets of parameters. In all cases, the results showed excellent agreement with that of time-consuming CFD simulations.

6. Concluding remarks

An enhanced thermal conduction model for predicting natural as well as forced convection dominated solid–liquid phase change was developed. The main feature of the model is to predict (1) the overall thermal behavior of the system and (2) the phase front position without recurring to the full solution of the Navier–Stokes equations. The model rests entirely on the conduction equation for both the solid and liquid phases. The effect of convection in the melt is mimicked via an enhanced conductivity that depends on the dimensionless numbers and the geometry of the flow.

The model was tested and confronted to full CFD solutions for a freezing duct flow problem and for buoyancy driven melting in an enclosure. In both cases, the predictions of the enhanced conduction model showed very good agreement with those of the CFD model. In other words, the enhanced conduction model can handle adequately convection dominated phase change problems without the solution of the flow. Not only is the enhanced conduction model simpler to implement but its computer simulations run at least ten times as fast as those of the CFD model. As a result, the enhanced conduction model is well suited for controlling real-time solid–liquid phase change processes that occur in industrial applications as well as in latent heat thermal energy storage systems.

As a final word, one could always argue that more detailed CFD simulations or additional experimental data are required to fine tune the constants in the enhanced conduction model. We have seen, however, that the magnitude of these constants is of order one. Moreover, satisfactory results are achieved with a simple scale analysis only. Adjusting the constants improves the accuracy of the predictions. One must bear in mind however that the proposed enhanced conduction model is a conceptual *representation* of reality, not reality itself. It was developed specifically for practical applications that require real-time control systems, i.e., applications that cannot otherwise rely on time-consuming CFD simulations.

Acknowledgement

This work was supported by the Natural Sciences and Engineering Research Council of Canada (NSERC).

References

[1] H. Ettouney, H. El-Dessouky, A. Al-Ali, Heat transfer during phase change of paraffin wax stored in spherical shells, J. Solar Energy Eng. Trans. ASME 127 (3) (2005) 357–365.
[2] G. Hed, R. Bellander, Mathematical modelling of PCM air heat exchanger, Energy Buildings 38 (2) (2006) 82–89.
[3] S. Tarhan, A. Sari, M.H. Yardim, Temperature distributions in trapezoidal built in storage solar water heaters with/without phase change materials, Energy Convers. Manage. 47 (15–16) (2006) 2143–2154.
[4] A. Trp, An experimental and numerical investigation of heat transfer during technical grade paraffin melting and solidification in a shell-and-tube latent thermal energy storage unit, Solar Energy 79 (6) (2005) 648–660.
[5] Z. Zhang, X. Fang, Study on paraffin/expanded graphite composite phase change thermal energy storage material, Energy Convers. Manage. 47 (3) (2006) 303–310.
[6] J.-C. Hsu, T.-H. Fang, W.-J. Chang, Inverse modeling of a workpiece temperature and melting depth during microthermal machining by scanning thermal microscope, J. Appl. Phys. 100 (6) (2006) 064305.
[7] L. Gosselin, M. Lacroix, Heat transfer and banks formation in a slag bath with embedded heat sources, Int. J. Heat Mass Transfer 46 (14) (2003) 2537–2545.

[8] O. Tadrari, M. Lacroix, Prediction of protective banks in high temperature smelting furnaces by inverse heat transfer, Int. J. Heat Mass Transfer 49 (13–14) (2006) 2180–2189.
[9] A. Laouadi, M. Lacroix, Thermal performance of a latent heat energy storage ventilated panel for electric load management, Int. J. Heat Mass Transfer 42 (1999) 275–286.
[10] M. Gharebaghi, I. Sezai, Enhancement of heat transfer in latent heat storage modules with internal fins, Numer. Heat Transfer Part A 53 (2008) 749–765.
[11] H. Hu, S.A. Argyropoulos, Mathematical modelling of solidification and melting: a review, Model. Simul. Mater. Sci. Eng. 4 (1996) 371–396.
[12] V. Kumar, F. Durst, S. Ray, Modeling moving-boundary problems of solidification and melting adopting an arbitrary Lagrangian–Eulerian approach, Numer. Heat Transfer Part B 49 (2006) 299–331.
[13] Y.-J. Jan, T.W.-H. Sheu, A cell-by-cell, thermally driven, mushy cell tracking algorithm for phase-change problems in dendritic solidification, Numer. Heat Transfer Part B 52 (2007) 69–105.
[14] Y.-J. Jan, T.W.-H. Sheu, Z.-Y. Hsu, F.-P. Lin, On a mushy cell tracking method for simulating gallium melting, Numer. Heat Transfer Part B 51 (2007) 351–374.
[15] R. Kahraman et al., A simplified model for melting of ice with natural convection, Int. Commun. Heat Mass Transfer 25 (1998) 359–368.
[16] A. Bejan, Convection Heat Transfer, third ed., Wiley, New York, 2004.
[17] V.A.F. Costa, Unification of the streamline, heatline and massline methods for the visualization of two-dimensional transport phenomena, Int. J. Heat Mass Transfer 42 (1) (1998) 27–33.
[18] S.V. Patankar, Numerical Heat Transfer and Fluid Flow, McGraw-Hill, New York, 1980.
[19] Fluent Corp., Fluent Users' Guide, Fluent Press, New Hampshire, 2005.
[20] O. Bertrand, B. Binet, H. Combeau, S. Couturier, Y. Delannoy, D. Gobin, M. Lacroix, P. Le Quéré, M. Medale, J. Mencinger, G. Vieira, Melting driven by natural convection, a comparison exercise: first results, Int. J. Therm. Sci. 38 (1999) 5–26.
[21] A. Bejan, Analysis of melting by natural convection in an enclosure, Int. J. Heat Fluid Flow 10 (3) (1989) 245–252.
[22] C. Gau, R. Viskanta, Melting and solidification of a pure metal on a vertical wall, J. Heat Transfer 108 (1986) 174–181.
[23] C. Gau, R. Viskanta, Melting and solidification of a metal system in a rectangular cavity, Int. J. Heat Mass Transfer 27 (1) (1984) 113–123.
[24] F.P. Incropera, D.P. Dewitt, Fundamentals of Heat and Mass Transfer, fifth ed., Wiley, New York, 2002.